IEEE Access
Multidisciplinary | Rapid Review | Open Access Journal

Received May 12, 2022, accepted May 20, 2022, date of publication May 23, 2022, date of current version June 3, 2022.

Digital Object Identifier 10.1109/ACCESS.2022.3177666

Design of Air-Trenches/Holes Assisted Depressed-Core 12-Mode Fiber for Less MIMO Space Division Multiplexing

MIAOFANG ZHOU, PING JIANG, HUAJUN YANG, WEINAN CAIYANG, YAN QIN, AND YIFAN ZHENG

School of Physics, University of Electronic Science and Technology of China, Chengdu 610054, China

Corresponding author: Huajun Yang (yanghj@uestc.edu.cn)

This work was supported by the National Natural Science Foundation of China (NSFC) under Grant 11574042 and Grant 61271167.

ABSTRACT An air-trenches/holes assisted depressed-core few-mode fiber (AT-AH-DC-FMF) that features some asymmetrical air trenches, air holes and a depressed step-index core is proposed in this paper. The AT and DC can produce great contribution in separating the non-degenerated LP modes and spatial modes, thus suppressing the crosstalk efficiently. Based on AT and AH, the bending loss values of AT-AH-DC-FMF can be satisfied with the ITU-T recommendations of G. 654. The simulation results indicate that our proposed fiber can support 12 spatial modes with the effective index difference between adjacent LP modes (Δn_{eff}) larger than 1.03×10^{-3} and the effective index difference between adjacent spatial modes (δn_{eff}) larger than 1.24×10^{-4}. The broadband characteristics such as Δn_{eff}, δn_{eff}, chromatic dispersion and effective mode field area (A_{eff}) over the whole C and L band are comprehensively investigated. Moreover, fabrication methods and birefringence are detailed discussed. Our proposed AT-AH-DC-FMF possesses great potential to be applied to less multiple-input multiple-output (MIMO-less) space-division multiplexing (SDM), thus enlarging optical communication capacity and simplifying the system complexity.

INDEX TERMS Few mode fibers, optical fiber communications, space division multiplexing, broadband characteristics, holes-assisted fibers.

I. INTRODUCTION

With the widespread of big data and cloud computing, the amount of data tends to an explosive growth [1]. The current data centers and optical networks are rapidly reaching their ultimate capacity due to the nonlinear Shannon limit of single-mode fibers (SMFs) [2]–[4]. Space division multiplexing (SDM) systems based on multi-core fiber (MCF) and few-mode fiber (FMF) have been extensively investigated for their potential to overcome these looming communication bottlenecks [5]–[7]. However, the high-performance MCF with some characteristics such as high core density, low crosstalk and low loss simultaneously faces a large number of technical challenges in the design and manufacturing process. It is also challenging to efficient couple signals in and out after all cores are tightly packed in a MCF with a limited cladding size [8]. FMF with its relatively simple structure produces unique advantages in terms of manufacturing methods and connectivity with standard SMFs. In addition, FMF with broadband characteristics over a wide wavelength range can provide the opportunities for SDM compatible with the mature wavelength-division multiplexing (WDM) technique [9]. The most crucial issue encountered in FMF is the crosstalk among different modes [10]. Employing the multiple input multiple output (MIMO) processing at the receivers is one of the approaches to settle this issue [11]–[13]. But the complexity of MIMO increases nonlinearly with the number of propagation modes, thus resulting in the depleting of the digital signal processing (DSP) capacity and the consumption of electric power [14]. To simplify MIMO, it is necessary to design special weakly-coupled FMF whose effective index difference between non-degenerated propagate modes (Δn_{eff}) is larger than 10^{-3}. Moreover, MIMO can be eliminated by enlarging the effective index difference between adjacent degeneracy modes (δn_{eff}) to larger than 10^{-4}. This method would be well

The associate editor coordinating the review of this manuscript and approving it for publication was Md Selim Habib.

satisfied with short-reach transmission such as data centers and computer rooms as its advantages of simplify systems [15]–[17].

Recently, researchers have made a large number of attempts in terms of adjusting the effective index (n_{eff}) of higher-order mode to enlarge the effective index difference between adjacent non-degenerated and degeneracy modes [18]–[21]. For example, in [20], a hole-assisted graded-index 4 LP-modes fiber with Min Δn_{eff} as high as 1.94×10^{-3} is proposed. In [21], a 3 LP-mode ring core fiber with Min Δn_{eff} as high as 2.5×10^{-3} is designed. However, 4 × 4 MIMO facilities are still needed to recover their fourfold degeneracy modes. It has been reported in [2], [14], [15], [22] that elliptical core fibers can act as a polarization maintaining fiber (PMF) used for MIMO-free SDM systems. For example, in [15], a 10 polarization-maintaining PANDA ring-core fiber with min δn_{eff} of 1.29×10^{-4} has been proposed. In [2], 10 distinctive polarization modes with Min δn_{eff} of larger than 1.32×10^{-4} have been achieved in a FMF composed of a central circular-hole and an elliptical-ring core. However, drawback of high doping difficulty is induced in those PMF, due to its large core and cladding relative refractive index difference of up to 3%. In addition, the core region of most of the PMF stays at a small value, resulting in a smaller effective mode field area than other FMF. What's more, PMF with the minimum effective refractive index difference of larger than 1.32×10^{-4} can only be applied in a shorter distance transmission than that of other FMF. Therefore, designing a weakly-coupled FMF with low doping, enough modes, large effective mode field area, sufficient Δn_{eff}, sufficient δn_{eff} and stable comprehensive broadband characteristics for less MIMO SDM-WDM systems is urgent.

In this paper, we proposed an air-trenches/holes assisted depressed-core 12-mode fiber for 2 × 2 MIMO SDM systems. COMSOL Multiphysics and MATLAB are utilized for investigating the fiber performance. The main contents of this paper are as follows: (I) In section 2, the schematic topology and particularities of our proposed air-trenches/holes assisted depressed-core few-mode fiber (AT-AH-DC-FMF) are introduced. (II) In section 3, the δn_{eff}, Δn_{eff} dependence on the parameters of DC and AT are investigated to explain the roles of DC and AT for AT-AH-DC-FMF. Then the bending loss as a function of the parameters of AT and AH is calculated to help the bending loss values of AT-AH-DC-FMF to satisfy the ITU-T recommendations of G. 654. (III) In section 4, the geometrical birefringence and stress birefringence are analyzed. (IV) In section 5, to confirm the compatibility of our proposed AT-AH-DC-FMF with mature WDM technology, the broadband characteristics such as δn_{eff}, Δn_{eff}, A_{eff} and chromatic dispersion are comprehensively researched over the whole C and L band. (V) In section 6, the fabrication methods and feasibility of our proposed AT-AH-DC-FMF are briefly discussed.

II. SCHEMATIC TOPOLOGY AND THEORY

Fig. 1 is the schematic of our proposed AT-AH-DC-FMF which composes of a step-index core in the center with some surrounded asymmetric air holes and air trenches, and a circular pure SiO_2 cladding. A list of parameters are used to describe the geometric structure of AT-AH-DC-FMF, where r, d, θ, β, w and p are the core radius, the DC radius, the angles of air trenches along y-axis and x-axis, the width of air trenches and the radius of air holes, respectively. l is the distance between air holes and core. Three particularities of our design should be noted: (1) asymmetric air trenches lie closely to the core, which affects the symmetry of the mode fields and the effective index of guided modes directly, producing great contribution in separating the degenerated spatial modes and non-degenerated LP modes; (2) the AT and AH has the maximum refractive index difference to the core, thus it exhibits better capability in reducing the bending loss of higher-order LP modes; (3) compared with bow-tie and steering wheel-type ring structure FMF, our design without complex doping of multi-clad structures and the extreme short gap between special structure and core, thus avoiding the increase of manufacturing complexity.

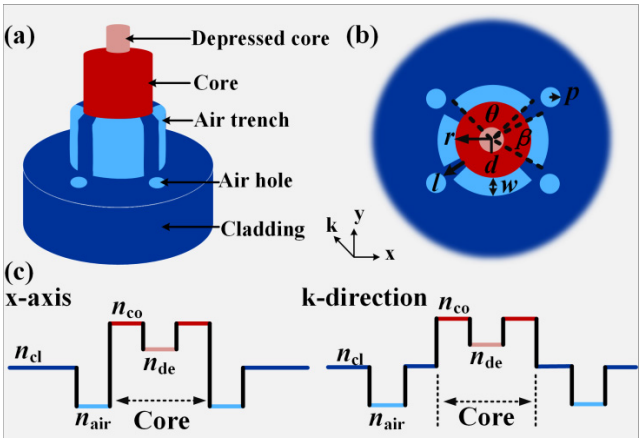

FIGURE 1. The schematic diagram and refractive index distribution of AT-AH-DC-FMF.

The refractive index profile of AT-AH-DC-FMF is shown in Fig. 1(c), where n_{co}, n_{de}, n_{cl} and n_{air} represent the refractive index of core, DC, cladding and air holes/trenches. The refractive index profiles in x-axis and k-direction are different as the exist of air trenches and air holes. We denote the refractive index difference $\Delta n_1 = n_{de} - n_{co}$. Correspondingly, $\Delta n_2 = n_{cl} - n_{co}$. In this paper, the core parameters with $r = 8.8$ μm, $\Delta n_1 = -0.2\%$ and $\Delta n_2 = -1.1\%$ support 7-LP-mode (LP_{01}, LP_{11}, LP_{21}, LP_{02}, LP_{31}, LP_{12} and LP_{41}) are employed. Then the detailed numerical simulations are carried out with a finite element mode solver (COMSOL Multiphysics) in the following sections. It has been pointed out in [23] and [24] that a detailed explanation of the analysis method is very important to prove the correctness of

a study. Therefore, we list the main simulation steps as follows: Firstly, establishing the model of our proposed AT-AH-DC-FMF with the "Wave optics" module of COMSOL Multiphysics. Secondly, setting up different materials for different regions of our proposed AT-AH-DC-FMF. Thirdly, setting up a perfectly matched layer (PML) at outmost region of the model to absorb the light escaping out the concerned region. Fourthly, dividing the grid with normal size. Finally, the simulation results can be achieved after the mode analysis.

III. FIBER PARAMETERS SELECTION

A. DC PARAMETERS

To highlight the importance of DC for our proposed AT-AH-DC-FMF, the min Δn_{eff} of the AT-AH-FMF is calculated and presented in the white region of Fig. 2 (that is $\Delta n_1 = 0$). As can be seen from this region, without DC, the min Δn_{eff} with its value of 0.86×10^{-3} appears between LP_{21} and LP_{02}, indicating that there is a higher possibility of coupling between LP_{21} and LP_{02} during the transmission. This phenomenon is consistent with the results in [5], indicating the correctness of our simulation method. Previous studies have shown that the n_{eff} of LP modes can be adjusted by changing the refractive index of the core region [5]. Therefore, a DC is added to the center of core to manipulate the n_{eff} between LP modes, to keep the min Δn_{eff} larger than the threshold value of 1×10^{-3}. The colormap of min Δn_{eff} between adjacent LP modes dependence on d and Δn_1 is presented in Fig. 2.

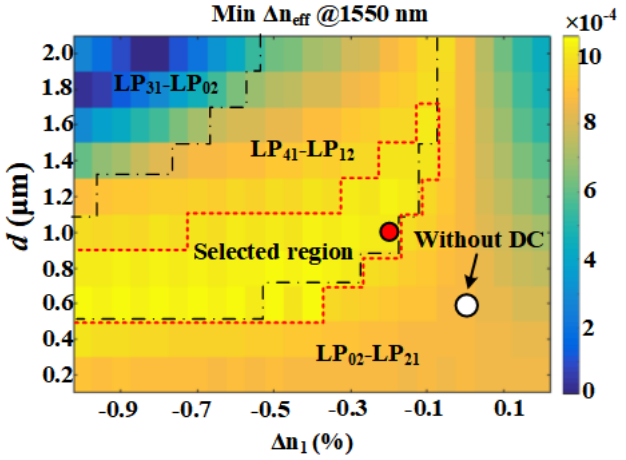

FIGURE 2. The min Δn_{eff} between adjacent LP modes as a function of d and Δn_1 at the wavelength of 1550 nm.

Fig. 2 shows the min Δn_{eff} between adjacent LP modes as a function of d and Δn_1 at the wavelength of 1550 nm. In Fig. 2, two black dotted lines indicate that with the variation of d and Δn_1, the min Δn_{eff} of our proposed AT-AH-DC-FMF appears between different adjacent LP modes. We circle the region that produces great contribution in separating the non-degenerated LP modes with red dotted line. In this region, the min Δn_{eff} between adjacent LP modes can be increased from initial 0.86×10^{-3} to 1.06×10^{-3}. In addition, the region with Δn_1 ranging from -1.0% to -0.1% and d ranging from 0.6 to 1.6 μm shows enough fabrication tolerances. Therefore, to apply our proposed AT-AH-DC-FMF to MIMO-less SDM systems, the parameters of DC (d and Δn_1) should be selected strictly according to our simulation results. Here, we determine parameters of the DC as $d = 1$ μm and $\Delta n_1 = -0.2\%$. At this time, the min Δn_{eff} is 1.02×10^{-3}.

B. AT/AH PARAMETERS

In this section, we aim to find out the optimum parameters of the air trenches, air holes and cladding, so as to achieve the 12-mode AT-AH-DC-FMF. Before setting out to do this work, the first thing we should notice is that the number of LP modes may be decreased after proper air trenches are added to our fiber. The main reason is that the air trenches affect the n_{eff} of LP mode, resulting in some n_{eff} of higher-order LP modes (LP_{12} and LP_{41}) being less than n_{cl}, which leads to the leakage of some higher-order LP modes. Traditionally, to increase the number of propagation modes, either the radius of core or the refractive index difference between the core and the cladding $|\Delta n_2|$ should be increased. However, the bending loss of the higher-order LP modes may still stay at a high value through this way, and the doping concentration will be increased. Considering the particular structure of our design, four air holes are added to the cladding to reduce the equivalent index of the cladding, so that the effective refractive index of LP_{12} and LP_{41} are larger than the equivalent index of the cladding. So the LP_{12} and LP_{41} can be bound in the core. Then the following steps are taken to select the optimum parameters of the air trenches, air holes and cladding: (1) in Fig. 3, investigating the impact of θ and β on Δn_{eff} and δn_{eff} of our proposed AT-AH-DC-FMF; (2) in Fig. 4(a-c), analyzing the influence of l, w and Δn_2 on the number of modes, min Δn_{eff} and min δn_{eff}; (3) in Fig. 4(d), exploring the relationship between the bending loss of AT-AH-DC-FMF, the width of air trenches and the radius of air holes.

To simultaneously keep Δn_{eff} larger than 1×10^{-3} and δn_{eff} larger than 1×10^{-4}, the θ and β should be selected strictly. We present the min Δn_{eff} between adjacent LP modes and the min δn_{eff} between adjacent spatial modes as a function of θ and β at the wavelength of 1550 nm in Fig. 3. In our simulation, we increase the angle β from 28 deg to 41 deg with a step size of 1 deg and the angles θ from 81 deg to 105 deg with a step size of 1 deg. From Fig. 3, it is obvious that the min Δn_{eff} increases with the increase of θ and β. In the region of 38 deg $\leq \beta \leq$ 41 deg and 96 deg $\leq \theta \leq$ 105 deg, Δn_{eff} is larger than 1×10^{-3}, however, δn_{eff} is smaller than 1×10^{-4}. In the region of 28 deg $\leq \beta \leq$ 33 deg and 82 deg $\leq \theta \leq$ 95 deg, δn_{eff} is larger than 1×10^{-4}, however, Δn_{eff} is smaller than 1×10^{-3}. Both regions should be excluded because they are inconsistent with the above requirements for Δn_{eff} and δn_{eff}. We circle the selected region that well satisfies the requirements for Δn_{eff} and δn_{eff} with a black dotted box. The selected region with θ ranging from 86 deg to 102 deg and β ranging from 31 deg to 40 deg

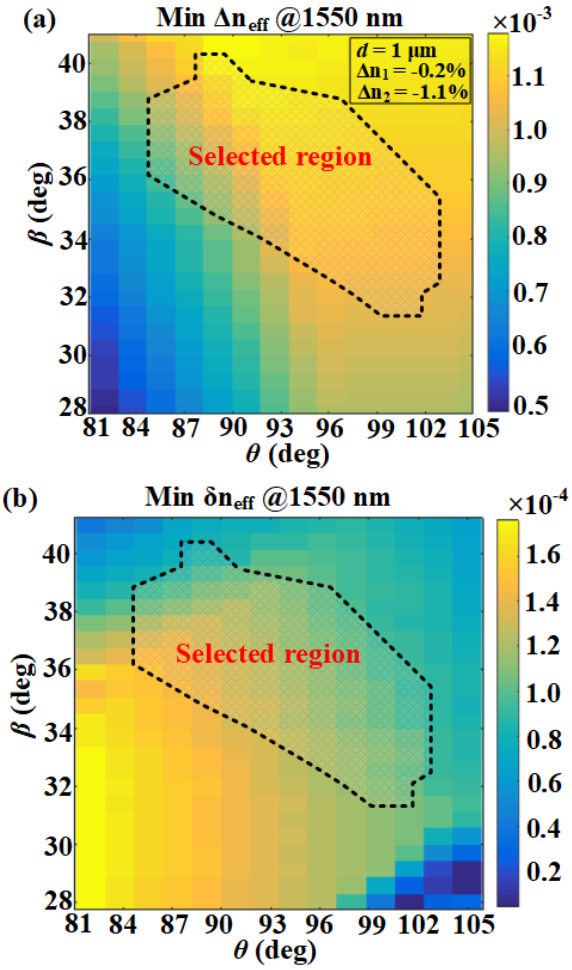

FIGURE 3. The min Δn_{eff} for adjacent LP modes and the min δn_{eff} for adjacent spatial modes depend on θ and β at 1550 nm.

indicates that our proposed AT-AH-DC-FMF possesses feasible fabrication tolerance during manufacturing air trenches. Finally, the parameters of air trench are fixed as $\theta = 88$ deg and $\beta = 36$ deg. At this time, the min $\Delta n_{eff} = 1.03 \times 10^{-3}$ and the min $\delta n_{eff} = 1.24 \times 10^{-4}$.

After the θ and β have been determined, the bending loss of our proposed AT-AH-DC-FMF can be controlled by adjusting the radius of air holes, the width of air trenches and the refractive index of cladding. To guarantee our proposed AT-AH-DC-FMF working over the C and L band, according to ITU-T recommendations G. 654, the bending loss of the highest-order mode (LP_{41}) should be lower than 0.5 dB/100 turns (the bending radius R = 30 mm) at 1625 nm [25]. In addition, the bending loss of the redundant mode (LP_{22}) (R = 140 mm) should be greater than 1 dB/m at 1530 nm [25]. Before setting out to get proper parameters for satisfying the requirements of bending loss, it is necessary for us to figure out the influence of the parameters of air holes, cladding and the width of air trenches on Δn_{eff}, δn_{eff}. Therefore, the influence of l, w and Δn_2 on the number of modes, min Δn_{eff} and min δn_{eff} are also explored in Fig. 4(a-c). Then the bending loss of AT-AH-DC-FMF as a function of the width of air trenches and the radius of air holes is investigated and the results are plotted in Fig. 4 (d).

Fig. 4(a,b) shows the min Δn_{eff} for adjacent LP modes and the min δn_{eff} for adjacent spatial modes as a function of l and w at the wavelength of 1550 nm, respectively. As can be seen from Fig. 4(a), the requirements of min Δn_{eff} and min δn_{eff} can be satisfied when l is larger than 1.6 μm, and the min Δn_{eff} and min δn_{eff} change slightly with the increase of l. In order to facilitate processing, we can choose l with a relatively larger value. Fig. 4(b) illustrates that the requirements of min Δn_{eff} and min δn_{eff} can be satisfied when w is ranging from 6.2 μm to 12.2 μm, and the min Δn_{eff} and min δn_{eff} change slightly with the increase of w. In Fig. 4(c), the number of modes can be increased with the increase of doping concentration. Five-modes fiber with min $\Delta n_{eff} = 1.98 \times 10^{-3}$ can be realized when $-0.5\% \leq \Delta n_2 \leq -0.1\%$. When $\Delta n_2 = -1.1\%$, 12 spatial modes are supported in our proposed AT-AH-DC-FMF with the min Δn_{eff} larger than 1.03×10^{-3} and the min δn_{eff} larger than 1.24×10^{-4}, respectively. When $\Delta n_2 \leq$ -1.2%, 14 spatial modes can be supported in our proposed AT-AH-DC-FMF. In this paper, we determine Δn_2 to -1.1%. Fig. 4(d) shows the bending loss of AT-AH-DC-FMF as a function of the width of air trenches and the radius of air holes. The orange solid line and orange dashed lines with circles correspond to the bending loss as a function of p at $w = 10.2$ μm. According to the orange dashed lines with circles, 7.9 μm $\leq p \leq$ 8.0 μm is required to keep the bending loss of unwanted mode (LP_{22}) larger than 1 dB/m (the bending radius R = 140 mm) at 1530 nm. The orange solid line with circles indicate that 7.9 μm $\leq p \leq$ 8.0 μm is needed to keep the bending loss of the highest mode (LP_{41}) lower than 0.5 dB/100 turns (R = 30 mm) at 1625 nm. The blue solid and dashed lines with circle represent the bending loss as a function of w at $p = 7.9$ μm. It can be seen in these two lines that 10.2 μm $\leq w \leq$ 10.4 μm is needed to keep the bending loss of the highest mode(LP_{41}) is lower than 0.5 dB/100 turns (the bending radius R = 30 mm) at 1625 nm. Therefore, 7.9 μm $\leq p \leq$ 8.0 μm and 10.2 μm $\leq w \leq$ 10.4 μm is acceptable to help the bending loss values of AT-AH-DC-FMF to satisfy the ITU-T recommendations of G. 654.

The mode field distributions and electric field polarization directions (white arrow surface) for 12 spatial modes (LP_{01}, LP_{11a}, LP_{11b}, LP_{21a}, LP_{21b}, LP_{02}, LP_{31a}, LP_{31b}, LP_{12a}, LP_{12b}, LP_{41a}, LP_{41b}) at 1550 nm are presented in Fig. 5.

It is worth noting that in the core regions without air trenches around, its ability to bound light is weaker than that of the core regions with air trenches around, thus resulting in a little energy leakage into the cladding. But it does not affect the normal use of our proposed AT-AH-DC-FMF.

IV. BIREFRINGENCE

Birefringence analysis of an optical fiber with an asymmetric refractive index distribution is necessary [5], [19]. Our proposed AT-AH-DC-FMF with asymmetrical air holes/trenches

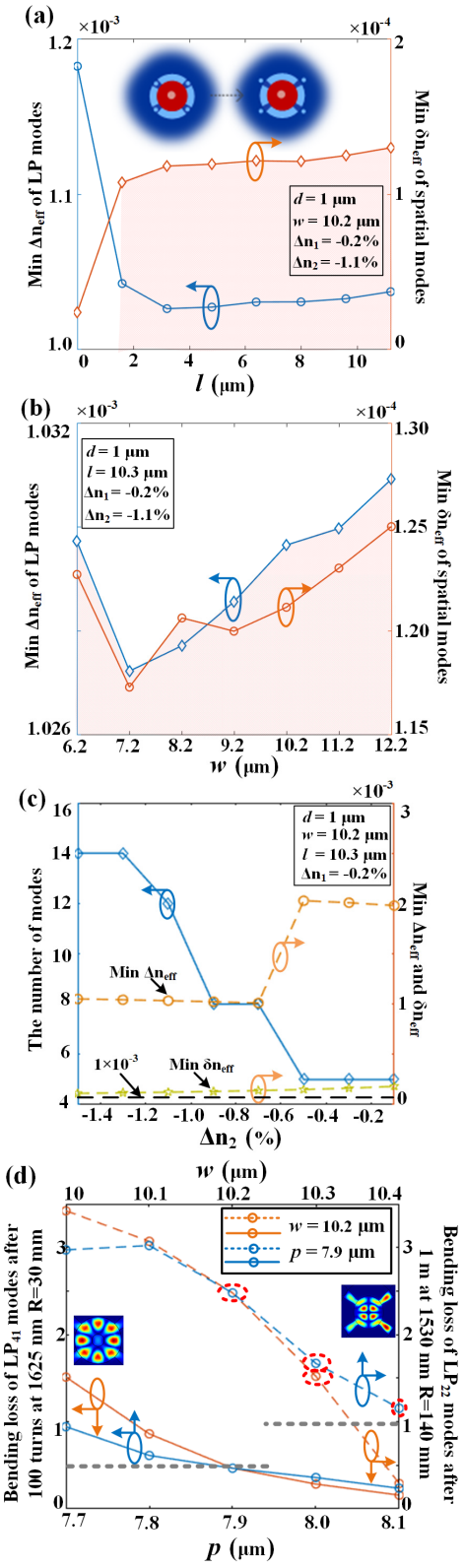

FIGURE 4. (a,b) The min Δn_{eff} for adjacent LP modes and the min δn_{eff} for adjacent spatial modes as a function of l and w at the wavelength of 1550 nm, respectively. (c) The influence of Δn_2 on min Δn_{eff}, min δn_{eff} and the number of modes. (d) The bending loss of AT-AH-DC-FMF as a function of the width of air trenches and the radius of air holes.

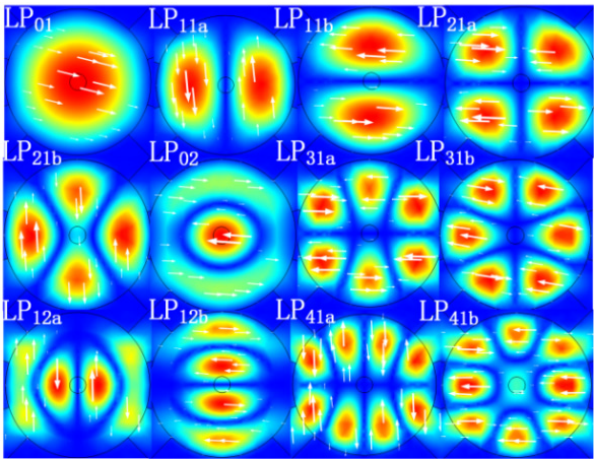

FIGURE 5. The mode field distributions and electric field polarization directions of 12 spatial modes in our optimized AT-AH-DC-FMF at 1550 nm.

TABLE 1. Elastic parameters used for modeling.

	Cladding	Core	DC
Thermal expansion coefficient α (1/K)	5.4×10^{-7}	1.01×10^{-6}	0.93×10^{-6}
Yong's modulus E (Pa)	72.5×10^{9}	68.26×10^{9}	69.02×10^{9}
Poisson's ratio ν	0.17	0.137	0.14288
Density ρ (kg/m^3)	2204	2244	2234
First stress optical coefficient B_1 (Pa^{-1})		6.5×10^{-13}	
Second stress optical coefficient B_2 (Pa^{-1})		4.2×10^{-13}	
Drawing temperature T_0 (°C)		1000	
Operating temperature T_1 (°C)		20	

in the x and y axis, so that the residual thermal stress components in the x and y directions are different, which may result in birefringence through the elasto-optical effect. After the material constants such as the Yong's modulus E, the Poisson's ratio ν, the thermal expansion coefficients α and material density ρ are determined, the birefringence analysis can be conducted with the "Structural Mechanics Module" of COMSOL Multiphysics. α of GeO_2 and SiO_2 are 7×10^{-6} (1/K) and 5.4×10^{-7} (1/K), respectively. α of a doped material can be expressed by mixture model shown as $\alpha = (1\text{-}m)\alpha_0 + m\alpha_1$ [26], where α_0 and α_1 are thermal expanding coefficient of the two kinds of dopants, $1-m$ and m denote the mole percentage of each dopant. The used elastic material parameters for modeling are calculated with the above method and listed in Table 1.

Birefringence consists of two components: geometrical birefringence (B_G) that is induced by irregular geometry and stress birefringence (Bs) that is related to thermal stress. The geometrical birefringence is defined as the difference between the n_{eff} of x-axis and y-axis, namely, $B_G = n^x_{eff} - n^y_{eff}$. The B_G of the eigenmodes LP_{01} is only 2.4×10^{-6}.

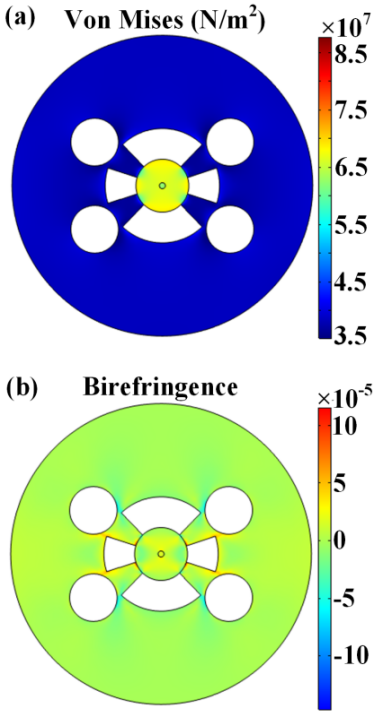

FIGURE 6. The Von Mises stress distribution and stress birefringence distribution on the transverse cross section of AT-AH-DC-FMF.

The stress birefringence is expressed as $Bs = \Delta c(\delta_x - \delta_y)$, where $\Delta c = 3.43 \times 10^{-12}$ m^2/N, δ_x and δ_y are the stresses along the x-axis and y-axis, respectively. Fig. 6 shows the Von Mises stress distribution and the stress birefringence on the transverse cross section of our proposed AT-AH-DC-FMF. The maximum Bs in the core region is only 5.6×10^{-5}. The average Bs is only 5.55×10^{-6} through calculating with integral formula [27]. Note that the Birefringence in our proposed AT-AH-DC-FMF is relatively small.

V. BROADBAND CHARACTERISTICS

In this section, the performance of AT-AH-DC-FMF (n_{eff}, Δn_{eff}, δn_{eff}, chromatic dispersion D and effective mode field area) covering the whole C and L band is investigated. The chromatic dispersion of AT-AH-DC-FMF is worth noting as it is a key factor resulting in optical pulse broadening. The chromatic dispersion D is composed of material dispersion D_m and waveguide dispersion D_w, both of which can be expressed as the following equations [13].

$$D = D_m + D_w \tag{1}$$

$$D_m = -\frac{\lambda}{c}\frac{\partial^2 n_m}{\partial \lambda^2} \tag{2}$$

$$D_w = -\frac{\lambda}{c}\frac{\partial^2 Re\,(n_{eff})}{\partial \lambda^2} \tag{3}$$

where c is the velocity of light in a vacuum, λ is the wavelength of light, n_m is the refraction index of material as a function of λ, $Re(n_{eff})$ is the real part of the n_{eff}, respectively. The hybrid Sellmeier equation [28] is applied to calculate the refraction index of SiO_2 and GeO_2-SiO_2 at different wavelengths. The differential mode delay (DMD) that is crucial for reduction of power consumption and complexity of MIMO processing is defined as follows (take LP_{nm} and LP_{01} as an example) [13].

$$\begin{aligned} DMD &= \tau_{LP_{nm}} - \tau_{LP_{01}} \\ &= \frac{n_{eff_{nm}} - n_{eff_{01}}}{c} - \left(\frac{\lambda}{c}\right)\left(\frac{\partial n_{eff_{nm}}}{\partial \lambda} - \frac{\partial n_{eff_{01}}}{\partial \lambda}\right) \end{aligned} \tag{4}$$

The n_{eff}, Δn_{eff}, δn_{eff}, chromatic dispersion and effective mode field area (A_{eff}) as a function of wavelengths are calculated and represented in Fig. 7.

The effective refraction index, Δn_{eff} and δn_{eff} as functions of wavelengths are investigated in Fig. 7(a) and 7(b). As can be seen from Fig. 7(a), asymmetric air trenches lie closely to the core, which affects the symmetry of the mode fields and the effective index of guided modes directly, thus leading to the n_{eff} of LP_{12} and LP_{41} is lower than the refraction index of cladding n_{cl}. But the AT and AH with enough size has the maximum refractive index difference to the core, exhibiting capability in reducing the equivalent index of the cladding. Therefore the LP_{12} and LP_{41} can still exist in the core. In Fig. 7(b), the min Δn_{eff} of LP modes is larger than 1×10^{-3}, thus the crosstalk between adjacent LP modes can be suppressed. In particular, as the min δn_{eff} larger than 1×10^{-4} over the whole C and L bands, the fourfold degenerate LP modes can be effectively separated into twofold modes, indicating our proposed AT-AH-DC-FMF has great potential to be applied to 2×2 MIMO SDM. Fig. 7(c) illustrates that the chromatic dispersions of all modes (except LP_{41}) increase slightly from conventional band to long-wavelength band. The difference among chromatic dispersion of different modes main caused by waveguide dispersion. That is, due to the particularity geometric structure of our proposed few mode fiber, the transmission path of C-L band light pulse in the few mode fiber is different, which affects the effective refractive index of the mode, and the effective refractive index of LP_{41} is the most affected. In the whole C and L band, the chromatic dispersion of all modes are lower than |60| ps/nm/km, which does not affect the normal use of our proposed AT-AH-DC-FMF in short-distance transmission. Even if we want to achieve dispersion-free propagation, dispersion-compensation techniques can be employed [29]. Fig. 7(d) shows the A_{eff} of spatial modes dependence on wavelengths. The A_{eff} of all spatial modes (except LP_{12b}) are larger than 100 μm^2 and the A_{eff} of all spatial modes (except LP_{41}) slightly changes with wavelength. The broadband characteristics over a wide wavelength range of covering the whole C and L bands indicate the compatibility of our proposed AT-AH-DC-FMF with the mature WDM technique.

The performance of our proposed AT-AH-DC-FMF depends on systematic variations of the fiber parameters that occur during the production process. So, we summarize the

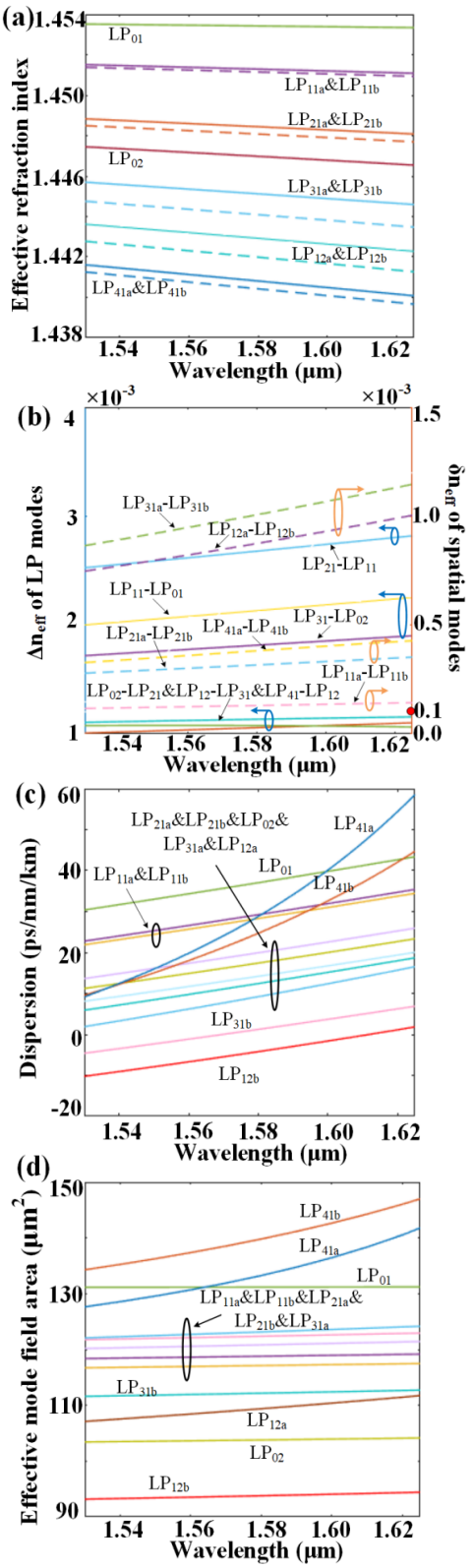

FIGURE 7. The (a) n_{eff}, (b) Δn_{eff} and δn_{eff}, (c) chromatic dispersions, and (d) A_{eff} of spatial modes as functions of wavelengths over the whole C and L band.

tolerance for Δn_{eff} and δn_{eff} of AT-AH-DC-FMF in Table 2. In this large range, the effective index difference between the effective index difference between adjacent LP modes (Δn_{eff}) is larger than 1×10^{-3} and the effective index difference between adjacent spatial modes (δn_{eff}) is larger than 1×10^{-4}. The enough tolerance shown in Table 2 indicates that our proposed few mode fiber has enough device robustness. Then the optimal fiber performance of AT-AH-DC-FMF is exhibited in Table 3, and the confinement losses (*CL*) of all modes are calculated with the following formula [7]:

$$CL = \frac{40\pi\, Im\,(n_{eff})}{\lambda \ln(10)} \tag{5}$$

where λ is the free-space wavelength and $\mathrm{Im}(n_{eff})$ is the imaginary part of the effective refractive index obtained by mode analysis. It can be seen in Table 3 that our optimal fiber shows great fiber performance, and especially, the bending loss of our proposed AT-AH-DC-FMF is lower than the bending loss in [5].

TABLE 2. The fabrication tolerance of AT-AH-DC-FMF.

r(μm)	Δn_1(%)	d(μm)	Δn_2(%)	θ(deg)	β(deg)	l(μm)
8.8	-1.0 to -0.1	0.6 to 1.6	-1.5 to -1.1	86 to 102	31 to 40	>1.6

VI. RECOMMENDATIONS FOR FABRICATION

Selecting an appropriate fabricating method can improve the probability of success during fiber fabrication. D. Chen *et al.* [30] used uniform air holes to form different basic cell structures for manufacturing triangular-hole photonic crystal fiber (PCF) and rectangular-hole PCF in practice, which provided an idea for manufacturing the AT in our proposed AT-AH-DC-FMF. Through this method, the structural distortion can be minimized during fabricating fiber with different shaped holes. According to mature technology in fabricating hole-assisted fibers [31], we believe the Stack-And-Draw technique is one of the ways that are suitable for the fabrication of our proposed AT-AH-DC-FMF. There are three steps that need to be followed to manufacture the AT-AH-DC-FMF. Firstly, some glass capillaries and glass rods are used to form AT and cladding. Secondly, 6% and 7.3% mole fraction of GeO_2 are needed to dope in SiO_2 to form the DC and core. Finally, our optimized AT-AH-DC-FMF can be manufactured after the melting and drawing process. The low doping during the manufacturing of DC and core indicates a relatively simpler fabrication process of our proposed AT-AH-DC-FMF than common elliptical core fibers and PMF. There is another method to fabricate our proposed AT-AH-DC-FMF. The main processes are as follows: firstly, fabricating a step-index core fiber preform with a circular pure SiO_2 cladding by utilizing the normal

TABLE 3. The optimal fiber performance of AT-AH-DC-FMF at 1550 nm.

	Fiber properties
n_{eff}	1.45348 (LP_{01}), 1.451411 (LP_{11a}), 1.451287 (LP_{11b}), 1.44868 (LP_{21a}), 1.44829 (LP_{21b}), 1.44726 (LP_{02}), 1.44547 (LP_{31a}), 1.44449 (LP_{31b}), 1.44334 (LP_{12a}), 1.44246 (LP_{12b}), 1.44129 (LP_{41a}), 1.44093 (LP_{41b})
Min δn_{eff} for spatial modes	1.24×10^{-4}
Min Δn_{eff} for LP modes	1.03×10^{-3}
A_{eff} (μm^2)	131.2 (LP_{01}), 118.5 (LP_{11a}), 116.9 (LP_{11b}), 122 (LP_{21a}), 120.4 (LP_{21b}), 103.6 (LP_{02}), 122.5 (LP_{31a}), 111.8 (LP_{31b}), 108 (LP_{12a}), 93.4 (LP_{12b}), 136.3 (LP_{41a}), 129.6 (LP_{41b})
Bending loss of spatial modes (R_b = 30 mm) (dB/100 turns)	<< 0.1 (LP_{01}), << 0.1 (LP_{11a}), << 0.1 (LP_{11b}), << 0.1 (LP_{21a}), << 0.1 (LP_{21b}), << 0.1 (LP_{02}), << 0.1 (LP_{31a}), << 0.1 (LP_{31b}), << 0.1 (LP_{12a}), << 0.1 (LP_{12b}), 0.068 (LP_{41a}), 0.012 (LP_{41b})
CL (dB/m)	$<<10^{-9}$ (LP_{01}), $<<10^{-9}$ (LP_{11a}), $<<10^{-9}$ (LP_{11b}), $<<10^{-9}$ (LP_{21a}), $<<10^{-9}$ (LP_{21b}), $<<10^{-9}$ (LP_{02}), $<<10^{-9}$ (LP_{31a}), $<<10^{-9}$ (LP_{31b}), 1×10^{-6} (LP_{12a}), 3.5×10^{-7} (LP_{12b}), 2.3×10^{-5} (LP_{41a}), 4.1×10^{-4} (LP_{41b})
DMD (ps/m)	-(LP_{01}), 6.69 (LP_{11a}), 7.32 (LP_{11b}), 14.79 (LP_{21a}), 16.51 (LP_{21b}), 18.53 (LP_{02}), 23.3 (LP_{31a}), 29.23 (LP_{31b}), 28.92 (LP_{12a}), 34.75 (LP_{12b}), 32.95 (LP_{41a}), 34.99 (LP_{41b})
Dispersion (ps/nm/km)	33.42 (LP_{01}), 25.73 (LP_{11a}), 24.83 (LP_{11b}), 16.52 (LP_{21a}), 14.07 (LP_{21b}), 10.91 (LP_{02}), 8.88 (LP_{31a}), -1.90 (LP_{31b}), 5.15 (LP_{12a}), -7.48 (LP_{12b}), 15.46 (LP_{41a}), 16.38 (LP_{41b})

MCVD technology; secondly, drilling the uniform air holes in particular positions of our fabricated preform to form the preform of our proposed AT-AH-DC-FMF; finally, our proposed few mode fiber can be fabricated after the drawing process. Previous study [32] provides us a method of filling nitrogen gas in the uniform air holes to against the ambient pressure, thus stopping the holes collapse during the fiber drawing. The discussion in this section proved that the design scheme of our proposed AT-AH-DC-FMF is feasible.

VII. CONCLUSION

In this paper, an AT-AH-DC-FMF features some asymmetrical air trenches, air holes and a depressed step-index core, supporting 12 spatial modes is proposed for MIMO-less SDM. The fiber performance dependence on the parameters of DC, AT and AH are investigated with FEM. According to our simulation results, the min Δn_{eff} of larger than 1.03×10^{-3} and min δn_{eff} of greater than 1.24×10^{-4} can be achieved with the help of AT and DC. The AT and AH plays an important role in helping the bending loss of AT-AH-DC-FMF satisfying the ITU-T recommendations of G. 654. Our proposed AT-AH-DC-FMF shows small birefringence effect and it is feasible to be fabricated with the Stack-And-Draw technique. In addition, stable comprehensive broadband characteristics such as small chromatic dispersion, large Δn_{eff}, large δn_{eff} and large effective mode area over the whole C and L band provide an opportunity for the MIMO-less SDM based on AT-AH-DC-FMF to be compatible with mature WDM technology, thus further enlarging optical communication capacity and simplifying the system complexity.

REFERENCES

[1] T. Yang, H. Zhang, L. Xi, Q. Li, X. Zhang, X. Wang, W. Zhang, and X. Tang, "Design of 18-mode hole-assisted elliptical-core polarization-maintaining few-mode fiber," *Opt. Commun.*, vol. 507, Mar. 2022, Art. no. 127647.

[2] J. K. Oh, Z. Feng, C. Zhao, R. Liao, S. Fu, P. P. Shum, and D. Liu, "Polarization-maintaining few mode fiber composed of a central circular-hole and an elliptical-ring core," *Photon. Res.*, vol. 5, no. 3, pp. 261–266, 2017.

[3] P. Sillard, D. Molin, M. Bigot-Astruc, H. Maerten, D. Van Ras, and F. Achten, "Low-DMGD 6-LP-mode fiber," in *Opt. Fiber Commun. Conf., OSA Tech. Dig.*, 2014, paper M3F.2.

[4] J. Zhang, G. Wang, H. Zhang, F. Wang, X. Yan, X. Zhang, S. Li, and T. Cheng, "A weakly-coupled few-mode optical fiber with a graded concave high-index-ring," *IEEE Photon. J.*, vol. 13, no. 2, pp. 1–10, Apr. 2021.

[5] Y. Xie, L. Pei, J. Zheng, Q. Zhao, T. Ning, and J. Li, "Design of steering wheel-type ring depressed-core 10-mode fiber with fully improved mode spacing," *Opt. Exp.*, vol. 29, no. 10, pp. 15067–15077, (2021.

[6] S. Jiang, L. Ma, Z. Zhang, X. Xu, S. Wang, J. Du, C. Yang, W. Tong, and Z. He, "Design and characterization of ring-assisted few-mode fibers for weakly coupled mode-division multiplexing transmission," *J. Lightw. Technol.*, vol. 36, no. 23, pp. 5547–5555, Dec. 1, 2018.

[7] M. Zhou, H. Yang, P. Jiang, W. Caiyang, Y. Qin, and B. Cao, "Design and analysis of hollow core Bragg fibers array for space division multiplexing," *Results Phys.*, vol. 30, Nov. 2021, Art. no. 104877.

[8] W. Song, H. Chen, J. Wang, C. Liu, Y. Chen, Z. Li, and M. Liu, "Panda type elliptical ring core few-mode fiber," *Opt. Fiber Technol.*, vol. 60, Dec. 2020, Art. no. 102361.

[9] S. Hong, K. Choi, Y. S. Lee, and K. Oh, "Two-mode fiber with a reduced mode overlap for uncoupled mode-division multiplexing in C+ L band," *Current Opt. Photon.*, vol. 2, no. 3, pp. 233–240, 2018.

[10] P. Sillard, D. Molin, M. Bigot-Astruc, A. Amezcua-Correa, K. de Jongh, and F. Achten, "50 μm multimode fibers for mode division multiplexing," *J. Lightw. Technol.*, vol. 34, no. 8, pp. 1672–1677, Apr. 15, 2016.

[11] Y. Jung, Q. Kang, H. Zhou, R. Zhang, S. Chen, H. Wang, Y. Yang, X. Jin, F. P. Payne, S.-U. Alam, and D. J. Richardson, "Low-loss 25.3 km few-mode ring-core fiber for mode-division multiplexed transmission," *J. Lightw. Technol.*, vol. 35, no. 8, pp. 1363–1368, Apr. 15, 2017.

[12] H. Zhang, J. Zhao, Z. Yang, G. Peng, and Z. Di, "Low-DMGD, large-effective-area and low-bending-loss 12-LP-mode fiber for mode-division-multiplexing," *IEEE Photon. J.*, vol. 11, no. 4, pp. 1–8, Aug. 2019.

[13] Y. Li, X. Wang, H. Zheng, X. Li, C. Bai, W. Hu, Y. Liu, and Q. Dong, "A novel six-core few-mode fiber with low loss and low crosstalk," *Opt. Fiber Technol.*, vol. 57, Jul. 2020, Art. no. 102211.

[14] S. Fu, Y. Wang, J. Cui, Q. Mo, X. Chen, B. Chen, M. Tang, and D. Liu, "Panda type few-mode fiber capable of both mode profile and polarization maintenance," *J. Lightw. Technol.*, vol. 36, no. 24, pp. 5780–5785, Dec. 15, 2018.

[15] H. Yan, S. Li, Z. Xie, X. Zheng, H. Zhang, and B. Zhou, "Design of PANDA ring-core fiber with 10 polarization-maintaining modes," *Photon. Res.*, vol. 5, no. 1, pp. 1–5, 2017.

[16] R. Maruyama, N. Kuwaki, S. Matsuo, and M. Ohashi, "Relationship between mode coupling and fiber characteristics in few-mode fibers analyzed using impulse response measurements technique," *J. Lightw. Technol.*, vol. 35, no. 4, pp. 650–657, Feb. 15, 2017.

[17] P. Sillard, M. Bigot-Astruc, and D. Molin, "Few-mode fibers for mode-division-multiplexed systems," *J. Lightw. Technol.*, vol. 32, no. 16, pp. 2824–2829, Aug. 15, 2014.

[18] J. Zhang, G. Wang, H. Zhang, F. Wang, X. Yan, X. Zhang, S. Li, and T. Cheng, "A weakly-coupled few-mode optical fiber with a graded concave high-index-ring," *IEEE Photon. J.*, vol. 13, no. 2, pp. 1–10, Apr. 2021.

[19] A. Corsi, J. H. Chang, R. Wang, L. Wang, L. A. Rusch, and S. LaRochelle, "Highly elliptical core fiber with stress-induced birefringence for mode multiplexing," *Opt. Lett.*, vol. 45, no. 10, pp. 2822–2825, 2020.
[20] J. Zhao, B. Li, M. Tang, S. Fu, S. Liu, P. P. Shum, and D. Liu, "Design and analysis of hole-assisted few mode fiber with ultra-low differential mode group delay (DMGD)," in *Proc. Asia Commun. Photon. Conf.*, vol. 2015, C. Lu, J. Luo, Y. Ji, K. Kitayama, H. Tam, K. Xu, P. Ghiggino, and N. Wada, Eds. Optical Society of America, 2015, paper ASu2A.68.
[21] M. Kasahara, K. Saitoh, and T. Sakamoto, "Design of three-spatial-mode ring-core fiber," *J. Lightw. Technol.*, vol. 32, no. 7, pp. 1337–1343, Apr. 1, 2014.
[22] S. Chen and J. Wang, "Design of PANDA-type elliptical-core multimode fiber supporting 24 fully lifted eigenmodes," *Opt. Lett.*, vol. 43, no. 15, pp. 3718–3721, 2018.
[23] C. A. Valagiannopoulos, "Semi-analytic solution to a cylindrical microstrip with inhomogeneous substrate," *Electromagnetics*, vol. 27, no. 8, pp. 527–544, Nov. 2007.
[24] C. Valagiannopoulos and A. Sihvola, "Limits for scattering resonances in azimuthally inhomogeneous nanotubes," *J. Opt.*, vol. 23, no. 12, Dec. 2021, Art. no. 125609.
[25] Y. Xie, L. Pei, J. Zheng, T. Ning, J. Li, B. Ai, and R. He, "Design and characterization of nanopore- assisted weakly-coupled few-mode fiber for simpler MIMO space division multiplexing," *IEEE Access*, vol. 8, pp. 76173–76181, 2020.
[26] R. Guan, F. Zhu, Z. Gan, D. Huang, and S. Liu, "Stress birefringence analysis of polarization maintaining optical fibers," *Opt. Fiber Technol.*, vol. 11, no. 3, pp. 240–254, Jul. 2005.
[27] Y. Liu, B. M. A. Rahman, and K. T. V. Grattan, "Thermal-stress-induced birefringence in bow-tie optical fibers," *Appl. Opt.*, vol. 33, no. 24, pp. 5611–5616, 1994.
[28] W. James Fleming, "Dispersion in GeO_2–SiO_2 glasses," *Appl. Opt.*, vol. 23, no. 24, pp. 4486–4493 1984.
[29] R. Noe, D. Sandel, and M. Yoshida-Dierolf, "Polarization mode dispersion compensation at 10, 20, and 40 Gb/s with various optical equalizers," *J. Lightw. Technol.*, vol. 17, no. 9, pp. 1602–1616, Sep. 1999.
[30] D. Chen, M.-L. Vincent Tse, and H.-Y. Tam, "Super-lattice structure photonic crystal fiber," *Prog. Electromagn. Res. M*, vol. 11, pp. 53–64, 2010.
[31] Y. Xie, L. Pei, J. Zheng, Q. Zhao, T. Ning, and J. Li, "Low-DMD and low-crosstalk few-mode multi-core fiber with air-trench/holes assisted graded-index profile," *Opt. Commun.*, vol. 474, Nov. 2020, Art. no. 126155.
[32] T. Yuan, X. Zhang, Q. Xia, Y. Wang, and L. Yuan, "A twin-core and dual-hole fiber design and fabrication," *J. Lightw. Technol.*, vol. 39, no. 12, pp. 4028–4033, Jun. 15, 2021, doi: 10.1109/JLT.2020.3022104.

MIAOFANG ZHOU was born in Hunan, China, in 1996. She is currently pursuing the Ph.D. degree with the University of Electronic Science and Technology of China. Her current research interests include few-mode fiber design, multi-core fiber design, optical design, and free space optical communication.

PING JIANG was born in Sichuan, China. She is currently an Associate Professor with the University of Electronic Science and Technology of China. Her current research interests include free space optical communication, optical design, and photonic crystal fiber design.

HUAJUN YANG was born in Sichuan, China. He received the Ph.D. degree, in 2007. From 2003 to 2004, he was a Senior Visiting Scholar with the School of Electronics and Computer Engineering, University of California, Santa Barbara. He is currently a Professor with the University of Electronic Science and Technology of China. His current research interests include few-mode fiber design, free space optical communication, optical design, and photonic crystal fiber design.

WEINAN CAIYANG was born in Yunnan, China. He is currently a Postdoctoral Researcher with the University of Electronic Science and Technology of China. His current research interests include omnidirectionally-emitting laser, free space optical communication, and optical design.

YAN QIN was born in Shanxi, China. She is currently pursuing the Ph.D. degree with the University of Electronic Science and Technology of China. Her current research interests include photonic crystal fiber design, vortex beam, turbulent atmosphere, and free space optical communication.

YIFAN ZHENG was born in Shanxi, China. She is currently pursuing the Ph.D. degree with the University of Electronic Science and Technology of China. Her current research interests include free space optical communication and optical design.